Spatiotemporal control of gene expression with pulse-generating networks

Subhayu Basu[†], Rishabh Mehreja[‡], Stephan Thiberge[†], Ming-Tang Chen[†], and Ron Weiss[†§¶]

[†]Department of Electrical Engineering, J-319, E-Quad, [‡]Department of Chemistry, Frick Laboratory, and [§]Department of Molecular Biology, Princeton University, Princeton, NJ 08544

Edited by Lonnie O'Neal Ingram, University of Florida, Gainesville, FL, and approved March 8, 2004 (received for review November 16, 2003)

One of the important challenges in the emerging field of synthetic biology is designing artificial networks that achieve coordinated behavior in cell communities. Here we present a synthetic multicellular bacterial system where receiver cells exhibit *transient* gene expression in response to a *long-lasting* signal from neighboring sender cells. The engineered sender cells synthesize an inducer, an acyl-homoserine lactone (AHL), which freely diffuses to spatially proximate receiver cells. The receiver cells contain a pulse-generator circuit that incorporates a feed-forward regulatory motif. The circuit responds to a long-lasting increase in the level of AHL by transiently activating, and then repressing, the expression of a GFP. Based on simulation models, we engineered variants of the pulse-generator circuit that exhibit different quantitative responses such as increased duration and intensity of the pulse. As shown by our models and experiments, the maximum amplitude and timing of the pulse depend not only on the final inducer concentration, but also on its rate of increase. The ability to differentiate between various rates of increase in inducer concentrations affords the system a unique spatiotemporal behavior for cells grown on solid media. Specifically, receiver cells can respond to communication from nearby sender cells while completely ignoring communication from senders cells further away, despite the fact that AHL concentrations eventually reach high levels everywhere. Because of the resemblance to naturally occurring feed-forward motifs, the pulse generator can serve as a model to improve our understanding of such systems.

synthetic biology | cell–cell signaling | gene regulation | feed-forward

Many biochemical processes in cells exhibit transient responses to long-lasting changes in environmental, intercellular, and intracellular conditions. These transient responses can have very different time scales that range from milliseconds to several hours and can also occur across different spatial dimensions. Examples can be found both in single cells and multicellular organisms, such as the adaptation of tumbling probabilities to nutrient levels in bacterial chemotaxis (1), bacterial flagellar development (2), somitogenesis protein expression during embryo development (3), JAK/STAT immune response pathways (4), circadian rhythms (5), and various feed-forward regulatory motifs (6). Despite the prevalence and importance of pulse behavior in naturally occurring systems, their operating principles are not well understood quantitatively. Building and studying synthetic networks that exhibit similar behavior can be helpful for an improved understanding of the principles and kinetics behind such spatiotemporal patterns in gene expression, as well as for engineering cellular systems for synthetic biology (7–18).

Recent studies have described small synthetic gene networks that can serve as model systems. These include the autorepressor (9), toggle switches (8, 14), the repressilator (10), the genetic clock (14), and digital logic gates (19).[‖] These efforts attempt to modify the behavior of individual cells to exhibit a desired response. However, it is also important to achieve coordinated behavior in multicellular environments. Toward this end, we engineered cell–cell communication in *Escherichia coli* (20) by using elements from the *Vibrio fischeri* quorum-sensing system (21).

In this paper, we present a synthetic multicellular bacterial system that integrates positive and negative regulation of gene expression to achieve a transient response to cell–cell communication. The system includes sender cells that can be induced to synthesize acyl-homoserine lactone (AHL), which then diffuses to nearby pulse-generating receiver cells. The receiver cells respond to this long-lasting increase in AHL concentration with transient expression of a GFP. The receiver circuit contains a feed-forward motif that in response to a stimulus exhibits an initial excitation followed by subsequent delayed inhibition (22). The circuit can also differentiate between various rates of increase in stimulus levels, enabling a spatiotemporal behavior where cells respond transiently to communication from nearby cells but ignore communication from cells that are further away.

Materials and Methods

Plasmid Construction. The sender plasmid pLuxI-Tet8 encodes an AHL synthase (LuxI) under the control of the promoter $P_{LtetO-1}$ (20). The pulse-generating receiver cells contain two plasmids, pLTSUB-202 and pPSSUB-101, or their variants. pLTSUB-202 encodes CI(LVA), a destabilized version of the CI repressor from bacteriophage λ (23), and enhanced cyan fluorescent protein (ECFP) under the control of $luxP_R$, although the ECFP is not used in the current study. This plasmid also encodes constitutive expression of LuxR from *V. fischeri* under the control of $luxP_L$. CI(LVA) was destabilized with a 12-aa *ssrA* tag (24). pLTSUB-202 was constructed from pINV-110-LVA (15) and pRCV-3 (25). pLTSUB-202 contains a kanamycin resistance marker and a p15A replication origin. pLTSUB-202-RBSD (RBS, ribosome-binding site) and pLTSUB-202-RBSH differ from pLTSUB-202 in the RBS located upstream of *cI* coding region, resulting in weaker translation efficiency (RBS II for *cI* in pLTSUB-202 is stronger than RBS D, which is stronger than RBS H). The different ribosome binding sites were chosen based on our previous studies (25) and were integrated by using PCR primers. pPSSUB-101 (chloramphenicol resistance, ColE1 replication origin) contains a destabilized version of GFP [GFP(LVA) from pGFP(LVA), Clontech] under the control of a novel hybrid promoter $luxP_RcI\text{-}O_R1$ that consists of the wild-type $luxP_R$ promoter with a CI O_R1 operator site inserted at the +1 transcription start (25). This promoter was constructed by encoding O_R1 on PCR primers and inserting it after $luxP_R$. pPSSUB-101-mut4 is a variant of pPSSUB-101 with a single base C → A mutation in the fourth base of O_R1 to reduce repressor/operator affinity (25). pPSSUB-101 was made from pRKM-102 (25) and pLuxI-Tet8. The Stratagene QuikChange kit was used for the operator mutation. We used restriction enzymes and T4

This paper was submitted directly (Track II) to the PNAS office.

Abbreviations: AHL, acyl-homoserine lactone; RBS, ribosome-binding site.

¶To whom correspondence should be addressed. E-mail: rweiss@princeton.edu.

‖Weiss, R. & Basu, S., First Workshop on Non-Silicon Computing, Feb. 13, 2002, Boston, MA.

DNA ligase (New England Biolabs), and PCR SuperMix High Fidelity (Invitrogen).

Data Acquisition and Analysis. *E. coli* strain DH5α (λ-, recA1-) (*E. coli* Genetic Stock Centre strain 7855) was used for the pulse-generator experiments. Cells transformed with the appropriate plasmids were grown at 37°C in M9 minimal media (Difco) supplemented with 0.2% casamino acids, 200 μM thiamine, 100 μM $CaCl_2$, appropriate antibiotics of 50 μg/ml kanamycin (Shelton Scientific, Shelton, CT) and 25 μg/ml chloramphenicol (EM Science), and inducers as indicated in the text. For the liquid experiments, expression was induced at an early log phase (OD_{600} of 0.1) by the addition of AHL ($3OC_6HSL$, Sigma-Aldrich) at the appropriate concentration. One-milliliter samples were taken every 5 min and immediately analyzed by fluorescence-activated cell sorting. Fluorescence data were recorded by using a Beckman Coulter Cytomics FC 500 Series flow cytometer and a Beckman Coulter Altra, both with a 488-nm argon excitation laser and a 515- to 545-nm emission filter, and calibrated by using SPHERO Rainbow Calibration Particles (RCP-30-5A, Spherotech). For each sample, 50,000 events were collected. Cultures were maintained at OD_{600} densities between 0.1 and 0.3 by repeated dilutions. WINMDI (The Scripps Research Institute, La Jolla, CA) and MATLAB (The MathWorks, Natick, MA) software was used for data analysis.

For the solid-phase experiment, time-lapse microscopy was conducted on a Zeiss Axiovert 200M microscope equipped with a cooled ORCA-ER charge-coupled device camera (Hamamatsu, Middlesex, NJ). A receiver culture was grown to OD_{600} of 0.1 in M9 liquid media, concentrated 4-fold, and spread evenly on an M9 agar slide. A sender culture was grown simultaneously to OD_{600} of 1.0 in M9 liquid media, concentrated 20-fold, spotted with a single droplet on the same slide, covered with a coverslip, and sealed. The temperature of the samples was maintained at 37°C by using a Zeiss incubation system. Brightfield and fluorescence images at different distances from the senders were captured with a 63× PH3 oil objective every 4 min by using custom software. Images were analyzed by using MATLAB software to obtain normalized average cell fluorescence for any given field of view.

Models. Two models were constructed to simulate the system behavior. The first model was used to analyze single cell response to variations in inducer concentrations and the kinetic parameters of genetic elements. The second model also included a spatial component to simulate AHL diffusion and cell–cell communication on solid-phase media. Both models were based on ordinary differential equations and were simulated by using MATLAB, as described in *Supporting Text* and Table 1, which are published as supporting information on the PNAS web site. A stochastic model (26) was also developed to investigate gene expression noise, but the simulations yielded the same average behavior with no qualitative differences (data not shown).

Results

Network Design. The two networks in Fig. 1 depict the genetic circuits for sender cells that synthesize the AHL inducer and receiver cells that exhibit the pulse response. To initiate cell–cell communication from the sender cells, the LuxI synthase from *V. fischeri* (21) is expressed under the control of the $P_{LtetO-1}$ promoter (20). The LuxI synthase catalyses the production of AHL, which then freely diffuses from the senders to the receivers. The pulse-generator circuit comprises a LuxR protein downstream of the $luxP_L$ promoter, CI(LVA) controlled by $luxP_R$ promoter, and GFP(LVA) under the control of $luxP_RcI\text{-}O_R1$ (sequence available in *Plasmids* of

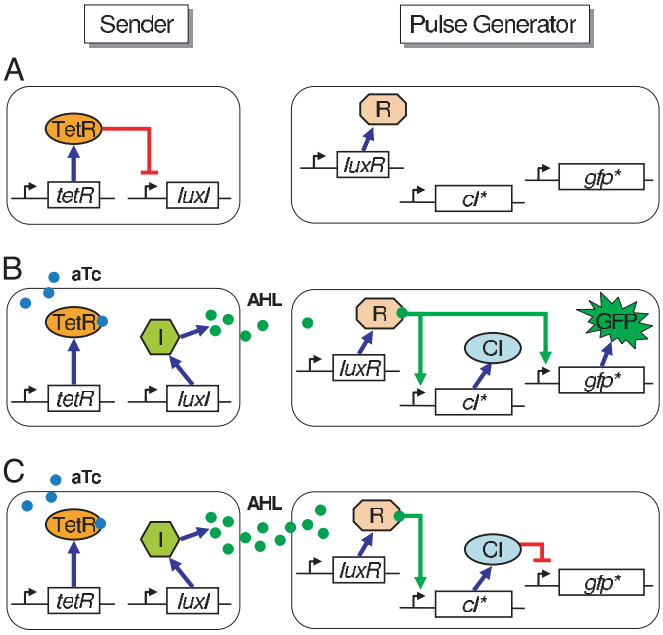

Fig. 1. Engineered sender cells are instructed to communicate a signal to the pulse-generating cells, which respond with transient expression of a fluorescent protein. TetR, I, R, CI, and GFP represent the protein products of the *tetR*, *luxI*, *luxR*, *cI**, and *gfp** genes, respectively, where * denotes a destabilized version of the protein. (*A*) Initially, no communication is taking place between the sender and pulse-generating cells. (*B*) Addition of anhydrotetracycline (aTc) instructs the sender cells to transmit the AHL signal to the pulse-generating cells, which in turn respond by expressing GFP and CI. (*C*) Continuous transmission of the AHL signal ultimately results in CI concentrations above the threshold required to repress GFP. The fluorescence disappears as GFP decays quickly.

Supporting Text and Figs. 6 and 7, which are published as supporting information on the PNAS web site). Transcription of both CI and GFP is activated by the LuxR-AHL dimer binding the *lux* box of the $luxP_R$ promoter. Once CI accumulates in sufficiently high concentrations, it binds the hybrid $luxP_R$ promoter and inhibits further production of GFP. This race condition between GFP expression and CI build-up results in transient GFP expression in response to a long-lasting increase in AHL concentration. Before induction, there is a low basal level of GFP expression. Upon induction, GFP levels rise initially, then fall and settle to a low level (which may be higher or lower than the initial level).

Engineering and Analysis of Temporal Response. Our temporal simulations suggest that various pulse characteristics can be forward-engineered to obtain desired behavior (the model is described in detail in *Supporting Text* and Table 1). Key characteristics of a pulse include rise time, fall time, width, amplitude, and gain. Pulse gain is the difference between the maximum and the final steady state GFP values, divided by the final steady state GFP value. Fig. 2*a* shows the simulated effect of CI translation efficiency and repressor/operator binding affinity on pulse gain. With a high CI translation efficiency and operator binding affinity, GFP levels never rise. In this case, even without AHL, leaky CI expression completely represses $luxP_RcI\text{-}O_R1$. Low values for the parameters in Fig. 2*a* result in high GFP expression in response to AHL, with little subsequent repression. We used this analysis to guide us in constructing a small library of pulse-generator circuits with combinations of different CI translation and repressor efficiencies.

We tested our capacity to forward-engineer pulse character-

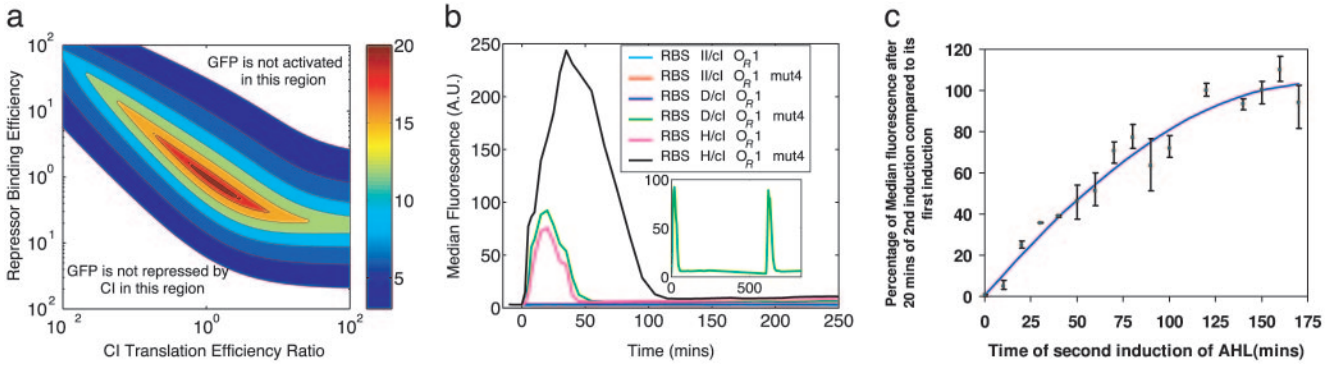

Fig. 2. Forward-engineering of pulse behavior. (*a*) Simulated contour map showing how the pulse gain changes with variations in CI RBS efficiency and repressor/operator affinity. (*b*) Experimental results of the circuit library showing median fluorescence-activated cell sorting fluorescence values of GFP measured every 2.5 to 5 min of different pulse-generator circuits in response to 140 nM AHL (*Inset* demonstrates the ability to completely regenerate the pulse a second time). (*c*) The refractory period of a pulse-generator circuit (RBS H, CI O_R1 mut4), as described in the text. The figure indicates average, low, and high fluorescence values for triplicate experiments.

istics by using this circuit library. Cultures of *E. coli* with different combinations of RBSs and operator sites were grown to an OD_{600} of 0.1, and then AHL was added to a final concentration of 140 nM. Culture samples were then assayed with fluorescence-activated cell sorting every 5 min to observe the time course of fluorescence (Fig. 2*b*). Cell cultures were repeatedly diluted with fresh media containing AHL to maintain cell density around an OD_{600} of 0.1–0.3. As seen in Fig. 2*b*, the circuit with the strongest RBS (RBS II) and original CI O_R1 did not produce a noticeable response. However, by combining the weakest RBS (RBS H) and the O_R1 single-base mutation we were able to obtain a pulse with high fluorescence and extended duration. Fig. 8, which is published as supporting information on the PNAS web site, shows representative flow cytometry population statistics of the pulse for this circuit combination. As evidenced by the experimental results, the precise magnitude of these kinetic rates determines the intensity and duration of the pulse and whether it will even function at all.

To ensure that AHL is not toxic to the cells at the relevant concentrations, we also induced cells that contained a similar circuit without CI, and they yielded a high level of fluorescence that remained constantly elevated (data not shown). We also verified that high CI levels are not toxic and do not interfere with high fluorescence intensities (data not shown).

Pulse Regeneration. To further characterize the dynamic properties of the circuit, we studied whether the system could be reset to its original state. In lieu of knowledge about exact protein concentrations, the system's state can be defined by the observed fluorescence in response to the stimulus. The extent to which the system has reverted back to its original state can then be measured by examining the pulse-regeneration capability. The first experiment (Fig. 2*b Inset*) used the circuit with RBS D and the O_R1 single-base mutation. After AHL induction for 4 h, cells were washed with new media thrice to remove AHL. The culture was grown for an additional 6 h in fresh media without AHL. Afterward, AHL was again added to a final concentration of 140 nM. As shown in Fig. 2*b Inset*, the second pulse reached the same intensity levels as the first pulse.

In another experiment, Fig. 2*c* shows the ability of the circuit to regenerate the pulse a second time as a function of the time elapsed past the first period of AHL induction. Cells were induced with 140 nM AHL for 6 h, then washed and resuspended in fresh media without AHL. Then, every 10 min, three separate 2-ml aliquots were removed and induced again with 140 nM AHL for 20 min. These triplicate fluorescence measurements are displayed as a percentage of the fluorescence achieved at the same relative time point during the first pulse. After ≈140 min, the circuit was able to regenerate a second pulse with approximately the same intensity as the first pulse.

The time interval after a sensed event during which the circuit does not respond to new incoming signals is defined as the *refractory period*. It corresponds to the time required by the system to revert back to its original state. This period is largely determined by the decay of CI because a high level of the repressor will reduce subsequent activation of GFP. It is also affected by the decay of LuxR-AHL dimers that activate expression of CI from $luxP_R$. Both CI and LuxR-AHL dimer concentrations are determined by the level of AHL. Hence, the initial AHL inducer concentration will also affect the refractory period of the system.

Responses to Different Input Concentrations and Rates. Another important characteristic of a pulse generator is its sensitivity to different input concentrations. Fig. 3*a* shows pulses generated by a range of AHL concentrations. For AHL concentrations >47 nM, the pulses appear to have the same initial rising slope and approximately the same maximum level. The maximum amplitude reached by all pulses occurs at ≈45 min after induction. It is interesting to note that in control circuits without CI inhibition, AHL concentrations of 4,700 nM elicit significantly stronger GFP expression than 140 nM (data not shown). However, higher AHL concentrations beyond 140 nM exhibit similar pulse response because of the stronger inhibition by CI that offsets the stronger $luxP_R$ activation.

In addition to the final AHL concentration, a striking property of the circuit is its ability to detect the rate of AHL increase. This rate was observed to play a significant role in determining the timing and maximum amplitude obtained by the pulse. Fig. 3 *b* and *c* shows the simulated and experimental responses of the circuit to different rates of increase of AHL, with all stimuli reaching a final concentration of 50 and 47 nM, respectively. The experimental and simulated results exhibit the same qualitative trends where lower rates of AHL increase result in reduced and delayed maximum pulse amplitudes.

We attribute this rate-sensing ability to the variable delay in repression introduced by the feed-forward motif. When the AHL increase rate is high, the initial buildup of both GFP and CI is high. Soon thereafter, CI quickly shuts down $luxP_RcI\text{-}O_R1$ activity. However, during this window of activity, GFP is produced in large quantities. The result is a pulse with short delay and high amplitude. In contrast, when the AHL increase rate is lower, the initial buildup of both GFP and CI is correspondingly lower. It therefore takes longer for CI to shut

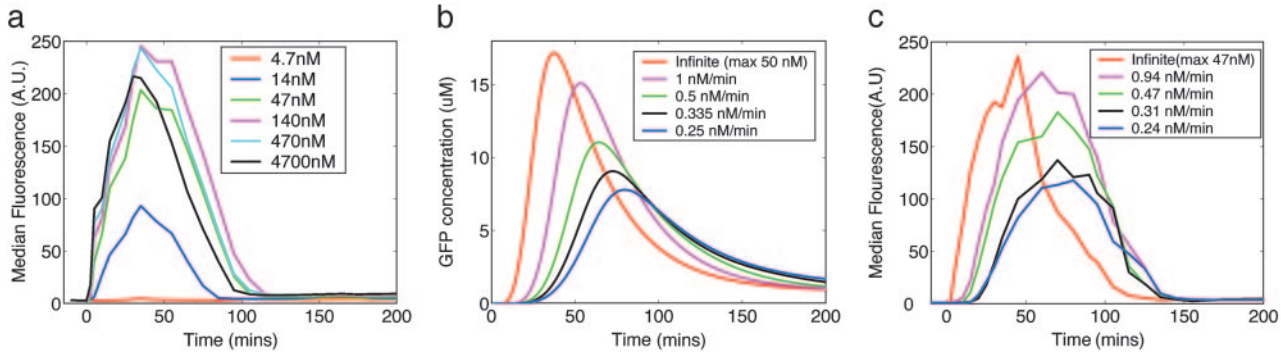

Fig. 3. The response of the pulse to different AHL concentrations and rates of increase. (*a*) Pulses resulting from different concentrations of AHL. The concentration of AHL was constant throughout the experiment. (*b*) Simulations graphing the time-series response to five different rates of AHL increase (all have a final AHL concentration of 50 nM). (*c*) Experimental results showing the median GFP fluorescence of separate cultures assayed by fluorescence-activated cell sorting with five different rates of AHL increase (all have a final concentration of 47 nM).

down $luxP_RcI\text{-}O_R1$. However, even with the longer delay, total GFP expression is lower because of the feed-forward component. This component consists of CI transcription, translation, dimerization, and operator binding. With lower transcription rates, CI transcription and translation dominate the delay incurred in repression. Dimerization and operator binding no longer play a significant role in the delay. Hence, for any given level of AHL during the buildup in inducer concentrations, CI repression of $luxP_RcI\text{-}O_R1$ will be higher than the previous case. Thus, GFP expression from $luxP_RcI\text{-}O_R1$ will be shut down at a lower concentration of AHL. This role of the feed-forward motif in the timing of CI repression and its overall effect on GFP accumulation was found in a time-based analysis of the relevant protein and occupied promoter concentrations, using the above simulations (data not shown).

Spatiotemporal Behavior. Because of the above rate response, communication from sender cells to pulse-generator cells deposited on a solid substrate elicits a response that depends on the distance between them. Specifically, receiver cells can differentiate between communication from nearby and far-away sender cells. Fig. 4 shows the first two of five positions in the microscope observations of circuit behavior on M9 agar slides. On average, cells that were closer to the senders began fluorescing earlier and displayed a pulse with a higher intensity than cells further away. Cells farthest from the senders (4.5 mm) did not display an observable response (Fig. 9*e*, which is published as supporting information on the PNAS web site). As a control, our previous experiments with a similar receiver circuit that did not contain CI exhibited increasing levels of GFP throughout the substrate (25).

The images in Fig. 4 and Movie 1, which is published as supporting information on the PNAS web site, revealed that neighboring cells exhibited wide variations in GFP responses. Fig. 9 provides single-cell time-series fluorescence data for all of the cells under observation in the different positions. The variations in liquid-phase fluorescence may be attributed to gene expression noise. However, the fluorescence distribution is wider in the solid-phase experiments than in the liquid-phase experiments (Fig. 8), likely because of heterogeneities in the local environments of the cells.

The delayed and reduced response was predicted by our spatiotemporal models. Fig. 5*a* shows the spatiotemporal pattern of GFP expression in the solid-phase experiment. The contour

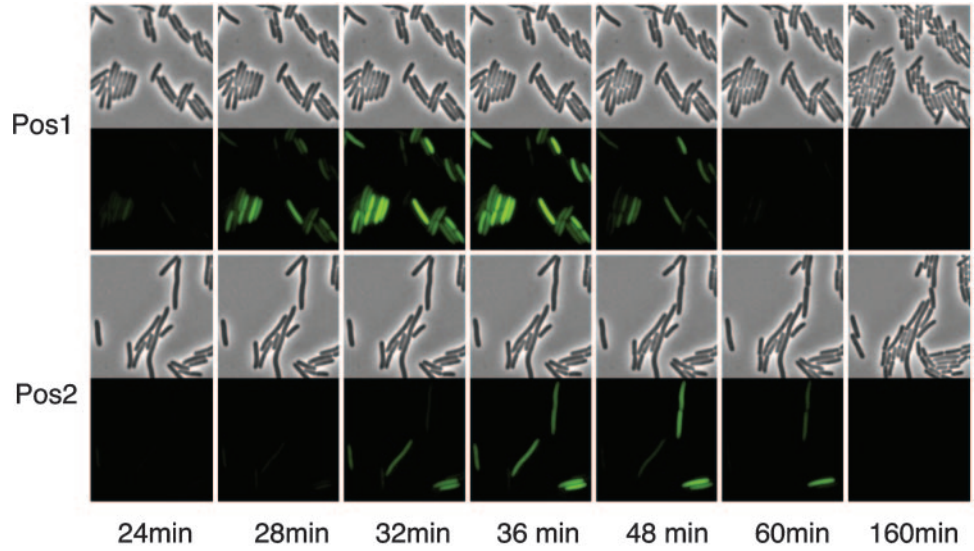

Fig. 4. Spatiotemporal behavior of the circuit. Time-series fluorescence and phase images of pulse-generating cells on an M9 agar slide at two different distances from the senders. Positions 1 and 2 are 2.5 and 3 mm away from the senders, respectively. These images are a cropped portion of the field of view in each position. For the cells shown in the cropped images, positions 1 and 2 cells achieved their highest average fluorescence at 32 and 36 min, respectively.

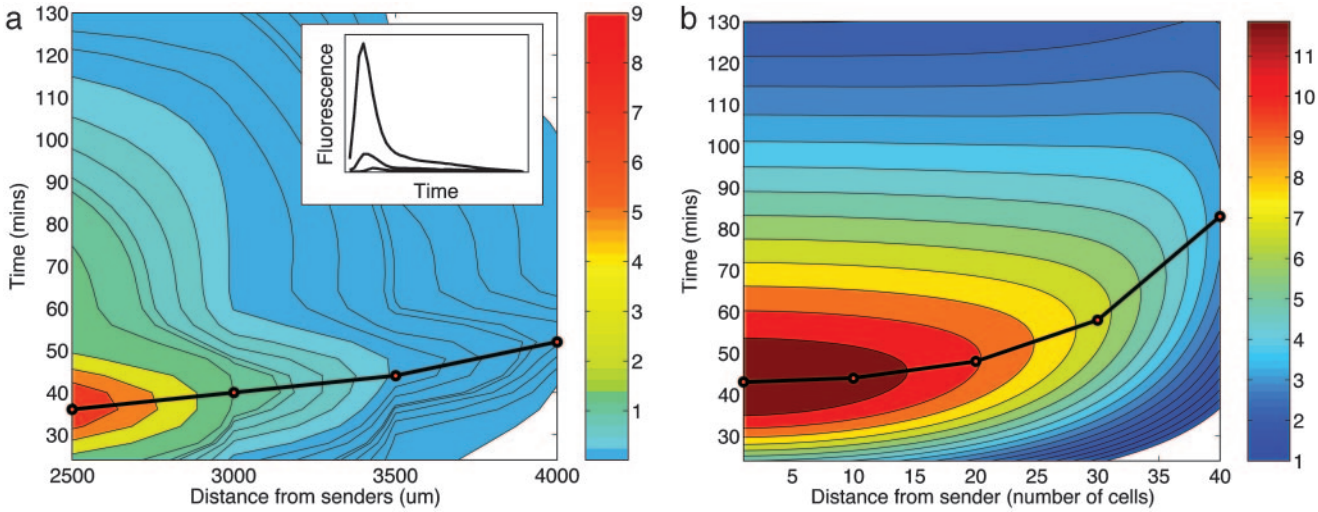

Fig. 5. Experimental and simulated spatiotemporal behavior of the pulse generator. Shown are contour maps of average fluorescence and simulated GFP concentrations at different distances from the senders over time. (*a*) Cells were tracked every 4 min in four different distances away from the senders (2.5, 3, 3.5, and 4 mm) for 130 min. The fluorescence observations (arbitrary units) at each position were fit with a second-order Gaussian curve and then used to compute the map with MATLAB contour function. *Inset* shows the time-series response at the first three positions. (*b*) A simulation of the spatiotemporal behavior of the pulse with cells placed on a 100 × 16-μm grid. A single sender cell was placed in the middle of the grid, and 50 receiver cells were placed linearly away from the sender. The simulation contour map shows the change in GFP levels (in μM) over time in the 20 receiver cells closest to the sender. The bold black lines in both figures connect the points of maximum amplitudes for the particular positions.

map relates distances from the senders on the horizontal axis and time on the vertical axis to GFP intensities. It was computed from the average GFP intensities of ≈500 cells per field of view at four different positions away from the senders during a 130-min pulse experiment. The contour map based on these observations highlights the diminished and delayed nature of the pulse as the distance from the senders increases. This behavior reflects the liquid-phase experimental results for different rates of AHL increase (Fig. 3) because on solid phase these rates are inversely correlated with distances from the senders. Fig. 5*a Inset* shows the time-series responses of the first three positions. The pulse at the last position was minimal, and cells at 4.5 mm from the senders did not display any observable response. The spatiotemporal simulation in Fig. 5*b* shows a corresponding qualitative trend.

Discussion

In this paper, we demonstrated and analyzed a multicellular bacterial system that we built *de novo* from simple and well characterized components. Within the operating thresholds of the pulse-generator circuit, a step increase in the concentration of the signaling molecule results in a pulse response with an amplitude that depends on the concentration of the signal. Interestingly, the amplitude and timing of the pulse differ when the signal concentration rises at different finite rates even when the final concentration is identical. Effectively, the engineered bacteria can sense the time derivative of the signal concentration. On solid media, the consequence of this particular feature is that receiver cells near the sender cells respond to the communication signal, whereas receiver cells that are further away ignore this signal. This behavior is possible despite the fact that AHL concentrations eventually reach high levels everywhere.

Models based on the characteristics of the simple components correctly predicted the overall system behavior both in liquid- and solid-phase media. Forward-engineering efforts to optimize system performance were guided by model predictions. They helped us choose between ribosome binding sites and operators with varying efficiencies such that the kinetic rates of the individual components were coupled more effectively (25). This process yielded a library of pulses with vastly different amplitudes, pulse gains, and durations. The simulation results also correlated well with the rate of increase and spatiotemporal experiments. Such correspondence has not only helped us understand the intricacies of the system, but can also provide additional guidance in designing future systems.

It may be possible to extend this system in a variety of ways. We are currently engineering the receiver cells to synthesize additional AHL in conjunction with GFP expression. This will help further propagate the original signal from the senders. A pulse-generator system with such a positive feedback loop resembles the network topology of the natural system responsible for the development of dorsal appendages in *Drosophila* (27). The two systems also share similar spatiotemporal patterns of gene expression (28). Another possible extension is to connect the output of the pulse generator as an input to a bistable switch (8), thereby generating a permanent fluorescent ring centered around the sender cells. Incorporating additional positive and negative feedback loops may increase the robustness of the circuit and reduce gene expression noise. Finally, in addition to the rational design of this circuit, we are exploring directed evolution techniques (15) to optimize the behavior of the system through protein engineering of CI, LuxR, and GFP.

Our pulse-generator system provides an important building block for the general purpose of engineering coordinated behavior in cell communities [e.g., amorphous computing (29) and pattern formation[††]]. As part of the emerging field of synthetic biology (30), such programmed coordinated behavior may have applications in a variety of fields including tissue engineering, biomaterial fabrication, and environmental sensing. In addition to its utility for synthetic biology, the analysis and experiments in this paper can improve the quantitative understanding of similar naturally occurring transcriptional regulatory networks. Similar feed-forward motifs are found in

[††]Nagpal, R., Proceedings of the Fourth International Conference on Complex Systems, June 9–14, 2002, Nashua, NH.

nature frequently, for example in organisms such as *E. coli* (22) and *Saccharomyces cerevisiae* (6), and in specific tasks in higher-level organisms such as somitogenesis (3) and JAK/STAT immune responses (4). Our study emphasizes how in addition to having the appropriate network topology, specific kinetic parameter values are required to achieve desired responses (e.g., optimal pulse gain). Another striking property of the circuit is its rate-sensing capability. Gradual increases in signaling molecule concentrations are more likely to occur in natural systems, and one should question whether certain systems respond to rates rather than actual concentrations. To address this and related questions, the pulse generator can serve as a model system to understand similar transient and spatiotemporal behaviors found in nature.

We thank F. Arnold, S. Tavazoie, D. Karig, and Y. Gerchman for helpful discussions and D. Karig for providing the software infrastructure for the simulations. This work was supported by Defense Advanced Research Planning Agency Biological Input/Output Systems Grant N66001-02-1-8929.

1. Falke, J. J., Bass, R. B., Butler., S. L., Chervitz., S. A. & Danielson, M. A. (1997) *Annu. Rev. Cell Dev. Biol.* **13,** 457–512.
2. McAdams, H. H. & Shapiro, L. (2003) *Science* **301,** 1874–1877.
3. Saga, Y. & Takeda, H. (2001) *Nat. Rev. Genet.* **2,** 835–845.
4. Hunter, T. (2000) *Cell* **100,** 113–127.
5. Dunlap, J. C. (1999) *Cell* **96,** 271–290.
6. Lee, T. I., Rinaldi, N. J., Robert, F., Odom, D. T., Bar-Joseph, Z., Gerber, G. K., Hannett, N. M., Harbison, C. T., Thompson, C. M. & Simon, I. (2002) *Science* **298,** 799–804.
7. Hasty, J., McMillen, D. & Collins, J. J. (2002) *Nature* **420,** 224–230.
8. Gardner, T., Cantor, R. & Collins, J. (2000) *Nature* **403,** 339–342.
9. Becskei, A. & Serrano, L. (2000) *Nature* **405,** 590–593.
10. Elowitz, M. & Leibler, S. (2000) *Nature* **403,** 335–338.
11. Hasty, J., McMillen, D., Isaacs, F. & Collins, J. J. (2001) *Nat. Rev. Genet.* **2,** 268–279.
12. Guet, C. C., Elowitz, M. B., Hsing, W. & Leibler, S. (2002) *Nature* **296,** 1466–1470.
13. Hasty, J., Dolnik, M., Rottschafer, V. & Collins, J. J. (2002) *Phys. Rev. Lett.* **88,** 148101-1–148101-4.
14. Atkinson, M. R., Savageau, M. A., Myers, J. T. & Ninfa, A. J. (2003) *Cell* **113,** 597–607.
15. Yokobayashi, Y., Weiss, R. & Arnold, F. H. (2002) *Proc. Natl. Acad. Sci. USA* **99,** 16587–16591.
16. Hasty, J., Isaacs, F., Dolnik, M., McMillen, D. & Collins, J. J. (2001) *Chaos* **11,** 207–220.
17. Weiss, R. (2001) Ph.D. dissertation (Massachusetts Institute of Technology, Cambridge).
18. Basu, S., Karig, D. & Weiss, R. (2002) *Nat. Comput.* **2,** 463–478.
19. Weiss, R., Homsy, G. E. & Knight, T. F., Jr. (1999) in *Evolution as Computation*, Natural Computing Series, eds. Landweber, L. F. & Winfree, E. (Springer, New York), pp. 275–295.
20. Weiss, R. & Knight, T. F., Jr. (2000) in *DNA Computing*, Lecture Notes in Computer Science, eds. Condon, A. & Rozenberg, G. (Springer, New York), Vol. 2054, pp. 1–16.
21. Bassler, B. L. (1999) *Curr. Opin. Microbiol.* **2,** 582–587.
22. Mangan, S. & Alon, U. (2003) *Proc. Natl. Acad. Sci. USA* **100,** 11980–11985.
23. Ptashne, M. (1986) *A Genetic Switch: Phage Lambda and Higher Organisms* (Cell Press and Blackwell Scientific, Cambridge, MA), 2nd Ed.
24. Andersen, J. B., Sternberg, C., Poulsen, L. K., Bjørn, S. P., Givskov, M. & Molin, S. (1998) *Appl. Environ. Microbiol.* **64,** 2240–2246.
25. Weiss, R., Basu, S., Kalmbach, A., Hooshangi, S., Karig, D., Mehreja, R. & Netravali, I. (2003) *Nat. Comput.* **2,** 47–84.
26. Gillespie, D. T. (1977) *J. Phys. Chem.* **81,** 2340–2361.
27. Shvartsman, S. Y., Muratov, C. B. & Lauffenburger, D. A. (2002) *Development (Cambridge, U.K.)* **129,** 2577–2589.
28. Muratov, C. B. & Shvartsman, S. Y. (2003) *Physica D* **186,** 93–108.
29. Abelson, H., Allen, D., Coore, D., Hanson, C., Homsy, G., Knight, T. F., Jr., Nagpal, R., Rauch, E., Sussman, G. J. & Weiss, R. (2000) *Commun. ACM* **43,** 74–82.
30. Ferber, D. (2004) *Science* **303,** 158–161.